Computers & Structures Vol. 25, No. 2, pp. 175–182, 1987
Printed in Great Britain.

0045-7949/87 $3.00 + 0.00
Pergamon Journals Ltd.

AXISYMMETRIC BUCKLING OF BIMODULUS THICK CIRCULAR PLATES

DAR-PING JUANG† and LIEN-WEN CHEN‡
Department of Mechanical Engineering, National Cheng Kung University, Tainan, Taiwan 700, Republic of China

(*Received* 13 *January* 1986)

Abstract—The static buckling of bimodulus thick circular and annular plates subjected to a combination of a pure bending stress and compressive stress is investigated. The thick finite element model, which includes the effect of transverse shear deformation, are created for axisymmetric buckling problems. The obtained results of buckling coefficient are compared with the exact solutions for ordinary thin plates. The accuracy of the finite element solutions are shown to be very good. The effects of various parameters on the buckling coefficients and neutral surfce locations are studied. The bimodulus properties are shown to have significant influences on the buckling coefficient.

NOTATION

R_i internal radius
R_0 external radius; radius for cirular plate
h plate thickness
$\mathbf{A}$ stretching stiffness matrix
$\mathbf{B}$ bending–stretchng coupling stiffness matrix
$\mathbf{D}$ bending stiffness matrix
$\mathbf{Q}$ material elastic matrix
Q_{ijk} plane-stress reduced stiffness coefficients
E^t, E^c respective tensile and compressive and Young's moduli
v^t, v^c respective tensile and compressive Poisson's ratios
G^t, G^c respective tensile and compressive shear moduli
G^{t*}, G^{c*} respective tensile and compresive transverse shear moduli
S transverse istropic parameter, $S = G^{t*}/G^t = G^{c*}/G^c$
$\mathbf{N}^0, \mathbf{M}^0, \mathbf{M}^{0*}$ initial stress and moment results
N_r buckling load, $N_r = hP_n$
K_{cr} buckling coefficients,

$$K_{cr} = \frac{N_r R_0^2}{E^c h^3/12(1 - v^{c^2})}$$

Z_n neutral surface position, $\epsilon_{rr} = 0$ and $\epsilon_{\theta\theta} = 0$
β ratio of bending stress to normal stress, $\beta = P_m/P_n$
P_n initial external normal stress
P_m initial external bending stress

INTRODUCTION

Recent investigations concerning composite materials have shown some composites to behave differently under simple tension and compression [1]. In addition to composite materials, some polycrystalline graphites and high polymers also behave differently in tension and compression [2]. This characteristic behavior, although actually curvilinear, is often approximated by two straight lines with a slope discontinuity at the origin. Thus they are called bimodulus materials (see Fig. 1).

It is believed that the first modern development of the basic constitutive equations of bimodulus materials was proposed by Ambartsumyan [3]. Bert [4] used the macroscopic material model [5] to study the laminated bimodulus composite plates. The bending analyses of bimodulus laminated rectangular plates are studied by Bert and his associates [6–8]. Bert *et al.* [9] are the first to study the vibration of thick rectangular bimodulus composite plates. Kamiya [10] treated large deflections of a circular plate by finite difference, and he also applied the energy method to large deflections of a rectangular plate [11]. Doong and Chen [12] investigated the axisymmetric initially stressed vibration of circular plate by using Galerkin method on the basis of Brunelle and Robertson [13]. The buckling problems appearing in the literature are sparse. Jones investigated the buckling of circular cylindrical shells [14] and stiffened multilayered circular cylindrical shells [15] on the basis of Ambartsumyan [3]. Doong and Chen [24] studied the buckling of thick bimodulus rectangular plates. No publication is to be found on the buckling of bimodulus circular and annular plates under a combination of bending stress and compressive stress.

In the present work, we employ the energy method to obtain the elastic and geometric stiffness matrix as indicated by Przemieniecki [16]. For the finite element model, the annular ring elements will be used and the Lagrangian polynomials other than Hermitian ones [17–19] are used to complete this work. The buckling coefficients for ordinary material (not bimodulus) circular plate obtained by present works are compared with the exact solutions [20]. The influence of various parameters on the neutral surface locations and the buckling coefficients of bimodulus plates are investigated.

† Graduate student.
‡ Professor.

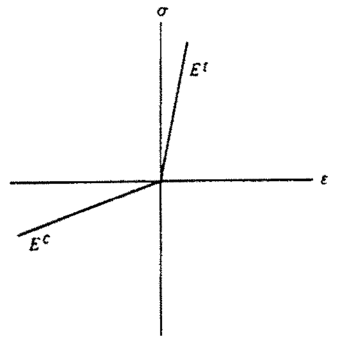

Fig. 1. Stress–strain relation of linearized different modulus material.

STRAIN ENERGY

The finite element stiffness matrices used in the displacement method of stability analysis can be derived most conveniently by starting with the non-linear strain–displacement equations. Following a technique described in [21, 22], the nonlinear strain–displacement equations, i.e. Green's strain tensor, in the cylindrical polar coordinate for the thick plate problems are as follows:

$$\begin{Bmatrix} \epsilon_{rr} \\ \epsilon_{\theta\theta} \\ 2\,\epsilon_{\theta z} \\ 2\,\epsilon_{rz} \\ 2\,\epsilon_{r\theta} \end{Bmatrix} = \begin{Bmatrix} \dfrac{\partial \xi_r}{\partial r} \\ \dfrac{1}{r}\dfrac{\partial \xi_\theta}{\partial \theta} + \dfrac{\xi_r}{r} \\ \dfrac{\partial \xi_\theta}{\partial z} + \dfrac{1}{r}\dfrac{\partial \xi_z}{\partial \theta} \\ \dfrac{\partial \xi_z}{\partial r} + \dfrac{\partial \xi_r}{\partial z} \\ \dfrac{\partial \xi_r}{r\partial \theta} + \dfrac{\partial \xi_\theta}{\partial r} - \dfrac{\xi_\theta}{r} \end{Bmatrix}$$

$$+ \begin{Bmatrix} \dfrac{1}{2}\left[\left(\dfrac{\partial \xi_r}{\partial r}\right)^2 + \left(\dfrac{\partial \xi_\theta}{\partial r}\right)^2 + \left(\dfrac{\partial \xi_z}{\partial r}\right)^2\right] \\ \dfrac{1}{2}\left[\left(\dfrac{\partial \xi_r}{r\partial \theta}\right)^2 + \left(\dfrac{\partial \xi_\theta}{r\partial \theta}\right)^2 + \left(\dfrac{\partial \xi_z}{r\partial \theta}\right)^2\right] + \left(\dfrac{\xi_r}{r}\dfrac{\partial \xi_\theta}{r\partial \theta} - \dfrac{\xi_\theta}{r}\dfrac{\partial \xi_r}{r\partial 2}\right) + \dfrac{1}{2}\left(\dfrac{\xi_r^2}{r^2} + \dfrac{\xi_\theta^2}{r^2}\right) \\ \left[\dfrac{\partial \xi_r}{r\partial \theta}\dfrac{\partial \xi_r}{\partial z} + \dfrac{\partial \xi_\theta}{r\partial \theta}\dfrac{\partial \xi_\theta}{\partial z} + \dfrac{\partial \xi_z}{r\partial \theta}\dfrac{\partial \xi_z}{\partial z}\right] + \left(\dfrac{\xi_\theta}{r}\dfrac{\partial \xi_r}{\partial z} - \dfrac{\xi_r}{r}\dfrac{\partial \xi_\theta}{\partial z}\right) \\ \left[\dfrac{\partial \xi_r}{\partial r}\dfrac{\partial \xi_r}{\partial z} + \dfrac{\partial \xi_\theta}{\partial r}\dfrac{\partial \xi_\theta}{\partial z} + \dfrac{\partial \xi_z}{\partial r}\dfrac{\partial \xi_z}{\partial z}\right] \\ \left[\dfrac{\partial \xi_r}{\partial r}\dfrac{\partial \xi_r}{r\partial \theta} + \dfrac{\partial \xi_\theta}{\partial r}\dfrac{\partial \xi_\theta}{r\partial \theta} + \dfrac{\partial \xi_z}{\partial r}\dfrac{\partial \xi_z}{r\partial \theta}\right] + \left(\dfrac{\xi_r}{r}\dfrac{\partial \xi_\theta}{\partial r} - \dfrac{\xi_\theta}{r}\dfrac{\partial \xi_r}{\partial r}\right) \end{Bmatrix}. \qquad (1)$$

The above strains can be denoted collectively by a column matrix

$$\mathbf{e}^T = \{e_{rr} e_{\theta\theta} e_{r\theta} e_{rz} e_{\theta z}\}$$

$$= \{\epsilon_{rr}\epsilon_{\theta\theta} 2\epsilon_{r\theta} 2\epsilon_{rz} 2\epsilon_{\theta r}\}, \qquad (2)$$

which can also be expressed as

$$\mathbf{e} = \hat{\mathbf{e}} + \mathbf{e}', \qquad (3)$$

where $\hat{\mathbf{e}}$ denotes the linear strains while $\mathbf{e}'$ denotes the nonlinear strains.

For the Mindlin plate theory, the displacements are assumed to be the following form

$$\xi_r(r, \theta, z) = u(r, \theta) + z\psi_r(r, \theta)$$
$$\xi_\theta(r, \theta, z) = v(r, \theta) + z\psi_\theta(r, \theta)$$
$$\xi_z(r, \theta, z) = w(r, \theta), \qquad (4)$$

where u and v are in-plane displacements and w is the lateral deflection of the neutral surface, while ψ_r and ψ_θ account for the effect of transverse shear.

The total potential energy of an elastic body is given as

$$\pi = U - \iiint_v B_i u_i \, \mathrm{d}V - \iint_s T_i^{(\nu)} u_i \mathrm{d}S, \qquad (5)$$

where U is the strain energy, B_i is the body force and $T_i^{(\nu)}$ is the surface traction. In the present problem the body force and surface traction are considered to be zero.

Let $\hat{\sigma}^0$ be the initial stress matrix and written as

$$\hat{\sigma}^0 = \begin{bmatrix} \hat{\sigma}_{rr}^0 & \hat{\sigma}_{r\theta}^0 \\ \hat{\sigma}_{r\theta}^0 & \hat{\sigma}_{\theta\theta}^0 \end{bmatrix}. \qquad (6)$$

Substituting equations (4) and (1) into equation (5) and neglecting higher order terms, the total potential energy due to the initial stresses is found to be

$$\pi = \frac{1}{2}\int_v [\mathbf{u}^T(\mathbf{E}^T + z\mathbf{F}^T)\mathbf{Q}(\mathbf{E} + z\mathbf{F})\mathbf{u}$$
$$+ \sum_{i=1}^{3} \mathbf{u}^T(\mathbf{G}_i^T + z\mathbf{H}_i^T)\sigma^0(\mathbf{G}_i + z\mathbf{H}_i)\mathbf{u}]\,\mathrm{d}V, \qquad (7)$$

where $\mathbf{Q}$ represents the reduced material elastic matrix of transversly isotropic elastic material. The detail of the matrices $\mathbf{E}$, $\mathbf{F}$, $\mathbf{G}_i$ and $\mathbf{H}_i$ can be seen in the appendix, and the displacement vector $\mathbf{u}$ is expressed as

$$\mathbf{u}^T = \{u, v, w, \psi_r, \psi_\theta\}. \qquad (8)$$

THE RITZ FINITE ELEMENT

For the finite element methods, the displacements can be expressed by the equation

$$\mathbf{u}_e = \sum_{j=1}^{n} \hat{\mathbf{u}}_{je}\mathbf{a}_{je}, \tag{9}$$

where the subscript "e" denotes that the variables are defined on the element, $\mathbf{a}_{je}$ are the shape functions and $\mathbf{u}_{je}$ is the nodal displacements to be determined.

Substituting equations (9) and (7) and subsequently applying the principle of minimum potential energy, we have

$$\frac{\partial \pi}{\partial \hat{\mathbf{u}}} = \mathbf{K}\hat{\mathbf{u}} = 0, \tag{10}$$

where $\mathbf{K}$ represents the stiffness matrix. $\mathbf{K}$ can be written as

$$\mathbf{K} = \mathbf{K}_E + \mathbf{K}_G, \tag{11}$$

where

$$\begin{aligned}\mathbf{K}_E &= \int_V (\hat{\mathbf{E}}^T + z\hat{\mathbf{F}}^T)\mathbf{Q}(\hat{\mathbf{E}} + z\hat{\mathbf{F}})\mathrm{d}V \\ &= \int_A [\hat{\mathbf{E}}^T\mathbf{A}\hat{\mathbf{E}} + (\hat{\mathbf{F}}^T\mathbf{B}\hat{\mathbf{E}} + \hat{\mathbf{E}}^T\mathbf{B}\hat{\mathbf{F}}) \\ &\quad + \hat{\mathbf{F}}^T\mathbf{D}\hat{\mathbf{F}}]\mathrm{d}A\end{aligned} \tag{12}$$

represents the elastic stiffness, and $\mathbf{A}$, $\mathbf{B}$ and $\mathbf{D}$ are extensional, flexural–extensional coupling and flexural stiffness matrices, respectively, and they are:

$$\begin{aligned}\mathbf{A} &= \int Q_{ij}\,\mathrm{d}z \\ \mathbf{B} &= \int zQ_{ij}\,\mathrm{d}z \\ \mathbf{D} &= \int z^2Q_{ij}\,\mathrm{d}z,\end{aligned} \tag{13}$$

in which the material elastic constants Q_{ij} are in the appendix, and while

$$\begin{aligned}\mathbf{K}_G &= \int_V \sum_i (\hat{\mathbf{G}}_i^T + z\hat{\mathbf{H}}_i^T)\hat{\sigma}^0(\hat{\mathbf{G}}_i + z\hat{\mathbf{H}}_i)\mathrm{d}\hat{V} \\ &= \int_A \sum_i [\hat{\mathbf{G}}_i^T\hat{\mathbf{N}}^0\hat{\mathbf{G}}_i + (\hat{\mathbf{G}}_i^T\hat{\mathbf{M}}^0\mathbf{H}_i \\ &\quad + \hat{\mathbf{H}}_i^T\hat{\mathbf{M}}^0\hat{\mathbf{G}}_i) + \hat{\mathbf{H}}_i^T\hat{\mathbf{M}}^{0*}\hat{\mathbf{H}}_i]\,\mathrm{d}A\end{aligned} \tag{14}$$

represents the geometric stiffness matrix. The matrices $\hat{\mathbf{N}}^0$, $\hat{\mathbf{M}}^0$ and $\hat{\mathbf{M}}^{0*}$ are defined by

$$\begin{aligned}\mathbf{N}^0 &= \int_{-h/2}^{h/2} \hat{\sigma}^0\mathrm{d}z \\ \mathbf{M}^0 &= \int_{-h/2}^{h/2} z\sigma^0\mathrm{d}z\hat{\sigma}\,\mathrm{d}z \\ \mathbf{M}^{0*} &= \int_{-h/2}^{h/2} z^2\hat{\sigma}^0\mathrm{d}z.\end{aligned} \tag{15}$$

It is noted that all the denotations $\hat{\mathbf{E}}$, $\hat{\mathbf{F}}$, $\hat{\mathbf{G}}_i$ and $\hat{\mathbf{H}}_i$ and $\hat{\mathbf{H}}_i$ represent the product of the one without hat "ˆ" and shape functions $\mathbf{a}_{i_e}$, and $\hat{\mathbf{u}}$ is the finite element nodal displacements. It has therefore been demonstrated that both the elastic and geometrical stiffness matrices can be determined from integrals of simple matrix products evaluated over the area. For bimodulus materials, the different properties in tension and compression cause a shift in the neutral surface away from the geometric midplane and thus symmetry about the midplane no longer holds. The result of this is that bending–stretching coupling, similar to orthotropic behavior, is exhibited. Thus, once the neutral surface has been determined, the $\mathbf{A}$, $\mathbf{B}$ and $\mathbf{D}$ are given in the next section. When the combined stiffness $\mathbf{K}$ has been determined, the equations of the present problem are then formulated as

$$(\mathbf{K}_E + \mathbf{K}_G)\hat{\mathbf{u}} = 0, \tag{16}$$

where $\hat{\mathbf{u}}$ is the finite element nodal displacements; these are homogeneous simultaneous equations.

Now, we put

$$\mathbf{K}_G = \lambda\mathbf{K}_G^*, \tag{17}$$

where λ is called the load factor and $\mathbf{K}_G^*$ is the relative reference of geometric stiffness due to intense initial stresses. Then, for nontrivial solutions of equation (16), the following relation must hold.

$$|\mathbf{K}_E + \lambda\mathbf{K}_G^*| = 0. \tag{18}$$

This equation represents the stability determinant. The smallest value of λ determines the instability condition for a specified loading configuration. The eigenvalue problems can be solved by means of any of the standard eigenvalue computer programs.

THE RING ELEMENT MODEL

The present paper will employ the finite strip to demonstrate the axisymmetric buckling problem. The advantages of finite strip are indicated in [23]; they include fewer data input, smaller matrix dimensions and more accurate solutions, etc. Thus the present problem will be simplified to a one-dimensional problem when we use ring elements to complete it.

In the present work, it is clear that $v = 0$, $\psi_0 = 0$ and $\partial/\partial\theta = 0$ in $\mathbf{E}$, $\mathbf{F}$, $\mathbf{G}_i$ and $\mathbf{H}_i$ for axisymmetric problems, and the Lagrangian polynomials will be used as shape functions, i.e.

$$\mathbf{u}^e = \sum_j \mathbf{a}_j * \hat{\mathbf{u}}_j, \tag{19}$$

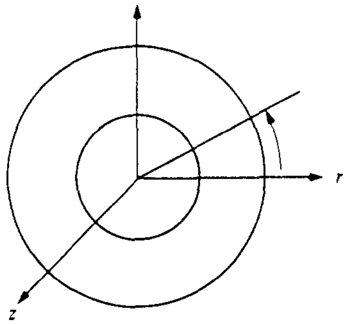

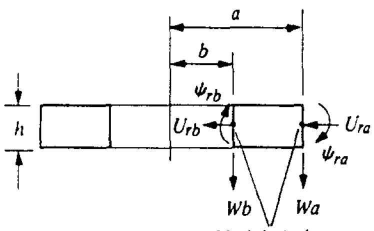

Fig. 2. Annular ring plate element and its generalized displacements.

where superscript "e" denotes element, the asterisk denotes element-by-element matrix multiplication,

$$\mathbf{a}_j^T = \{a_j a_j a_j\} \tag{20}$$

is the shape function vector and $\hat{\mathbf{u}}_j$ are the displacements of the corresponding nodal line j. For example, if we choose the ring elements with three nodal lines per element, the shape functions in one element are

$$a_1 = \frac{(r - r_2)(r - r_3)}{(r_1 - r_2)(r_1 - r_3)}$$

$$a_2 = \frac{(r - r_1)(r - r_3)}{(r_2 - r_1)(r_2 - r_3)}$$

$$a_3 = \frac{(r - r_1)(r - r_2)}{(r_3 - r_1)(r_3 - r_2)}, \tag{21}$$

where subscripts denote the sequential number in one element. The ring elements are shown in Fig. 2.

For a closed-form circular element, in order to avoid the problem of a singular point at a circular center, we let the circular element have a very small hole at center. It will be shown that this approach is very accurate in this paper.

Choosing the proper shape functions, the elastic stiffness $\mathbf{K}_E$ and geometric stiffness matrix $\mathbf{K}_G$ can be determined for each element; the element stiffness can be transferred into a global displacement system to solve the eigenvalue problem. Thus, we can complete the finite element stability analysis.

For bimodulus materials, it was indicated in the previous section that the symmetry about the mid-plane no longer holds because of the shift in the neutral surface away from the geometric midplane. To determine the Z-position of the neutral surface Z_n, one sets

$$\epsilon_{rr} = u_{,r} + Z_n \psi_{r,r} = 0, \tag{22}$$

which can be displayed at Gauss points. An iterative procedure is used to obtain the final displacement ratios. Thus we can give the **A**, **B** and **D** as [8, 9]

$$A_{ij} = \int_{-h/2}^{h/2} Q_{ij}\,dz = (Q_{ij2} + Q_{ij1})(h/2) + (Q_{ij2} - Q_{ij1})Z_n$$

$$B_{ij} = \int_{-h/2}^{h/2} zQ_{ij}\,dz = (Q_{ij1} - Q_{ij2})(h^2/8) + (Q_{ij2} - Q_{ij1})(Z_n^2/2)$$

$$D_{ij} = \int_{-h/2}^{h/2} z^2 Q_{ij}\,dz = (Q_{ij1} + Q_{ij2})(h^3/24) + (Q_{ij2} - Q_{ij1})(Z_n^2/3), \tag{23}$$

where subscripts "1" and "2" denote the tension and compression, respectively. For the transversly isotropic materials

$$Q_{33} = G_{r\theta} = G, \quad Q_{44} = k^2 G_{rz}, \quad Q_{55} = k^2 G_{\theta z},$$

where

$$G_{rz} = G_{\theta z} = G^* \text{ and } k^2 = \frac{\pi^2}{12}$$

is the shear correction factor.

RESULTS AND DISCUSSIONS

Consider an annular plate of uniform thickness h with inner radius R_i and outer radius R_0 in a state of initial stresses. The state of initial stresses on external edge is

$$P_r = P_n + 2zP_m/h, \tag{24}$$

where P_n and P_m are taken to be constants. It is comprised of a compression plus in-plane bending stress. The Lame's distribution is employed here, i.e. the stresses in terms of stress P_r can be shown to be

$$\hat{\sigma}_{rr} = -P_r \frac{R_0^2}{R_0^2 - R_i^2}\left(1 - \frac{R_i^2}{r^2}\right)$$

$$\hat{\sigma}_{\theta\theta} = -P_r \frac{R_0^2}{R_0^2 - R_i^2}\left(1 + \frac{R_i^2}{r^2}\right)$$

$$\hat{\sigma}_{r\theta}^0 = 0. \tag{25}$$

For convenient purpose, let

$$C_r = +\frac{R_0^2}{R_0^2 - R_i^2}\left(1 - \frac{R_i^2}{r^2}\right)$$

$$C_\theta = +\frac{R_0^2}{R_0^2 - R_i}\left(1 + \frac{R_i^2}{r^2}\right). \tag{26}$$

Thus the non-zero force and moment resultants in equation (15) are

$$\hat{N}_r^0 = -hP_nC_r,$$

$$\hat{N}_\theta^0 = -hP_nC_\theta$$

$$\hat{M}_r^0 = -h^2P_mC_r/6,$$

$$\hat{M}_\theta^0 = -h^2P_mC_\theta/6$$

$$M_r^{0*} = -h^3P_nC_r/12,$$

$$\hat{M}_\theta^{0*} = -h^3P_nC_\theta/12. \tag{27}$$

For the circular plate case, the Lame's distribution no longer holds, and the stresses are

$$\hat{\sigma}_{rr}^0 = \hat{\sigma}_{\theta\theta}^0 = -P_r \quad \text{and} \quad \hat{\sigma}_{r\theta}^0 = 0. \tag{28}$$

Thus the non-zero force and moment resultants in equation (15) become

$$N_r^0 = -hP_n,$$

$$N_\theta^0 = -hP_n$$

$$M_r^0 = -h^2P_m/6,$$

$$M_\theta^0 = -h^2P_m/6$$

$$M_r^{0*} = -h^3P_n/12,$$

$$M_\theta^{0*} = -h^3P_n/12. \tag{29}$$

Now, we put $\beta = P_m/P_n$, which represents the ratio of bending pressure to compression pressure, and also define the buckling coefficient K_{cr} as

$$K_{cr} = \frac{N_rR_0^2}{E^ch^3/12(1-\nu^{c2})}. \tag{30}$$

There are so many parameters that can be varied that it would be difficult to present results for all cases.

Only a few typical cases have been selected for discussion here. For verifying the accuracy of present results, the non-dimensional buckling coefficients of ordinary (not bimodulus material) thin circular plate are considered first. In Table 1, the present results for ordinary circular plate are compared with the exact

Table 1. Comparison between the present results and exact solutions in [20] for ordinary circular plates

R_0/h		8	10	20	50	100
Present results	K_{cr}	13.549	13.934	14.495	14.661	14.685
Exact solutions	K_{cr}	14.68	14.68	14.68	14.68	14.68

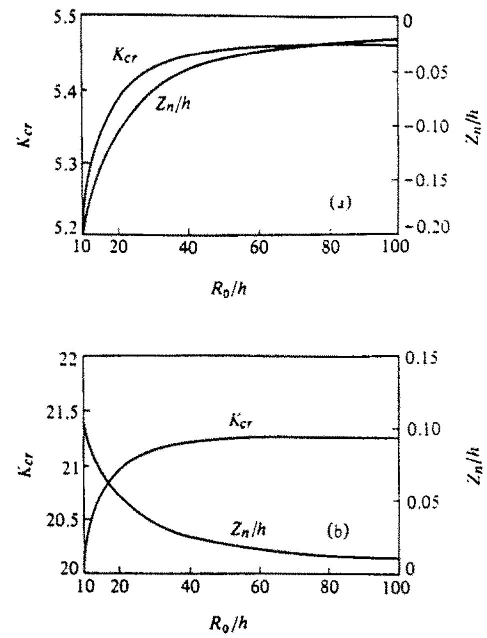

Fig. 3. Buckling coefficients and neutral surface locations of circular plate vs radius–thickness ratios for (a) $E^t/E^c = 0.2$ and (b) $E^t/E^c = 2.0$. $S = 1$; $\beta = 0$.

solution of thin plate by Timoshenko [20]. It can be shown that buckling coefficients with no bending stresses for ordinary plate which are calculated in the present paper coincide very well with Timoshenko's for clamped circular plate.

The buckling coefficients K_{cr} for the circular and annular plates are obtained in Figs 3–8. In the computations, $E^c = 1.0$, $\nu^c = 0.2$, $E^t/E^c = 0.2$–2.0 and ν^t is given by the relation

$$\nu^t = \nu^cE^t/E^c. \tag{31}$$

The shear moduli G^c and G^t in the respective compressive and tensile regions are

$$G^c = E^c/2(1+\nu^c), \quad G^t = E^t/2(1+\nu^t). \tag{32}$$

Plots of R_0/h vs K_{cr} and Z_n/h for circular plates are shown in Fig. 3 (a). The values of E^t/E^c, S and β are equal to 0.2, 1 and 0, respectively. It can be seen that the buckling coefficients increase with increasing values of R_0/h. Owing to the non-dimensional coefficient effect, the actual buckling load N_r which is equal to hP_n decreases with increasing radius to thickness ratio. The neutral surface locations of thick plates are further away from the middle plane than those of thin plates. The conditions in Fig. 3(b) are the same as those in Fig. 3(a) except that $E^t/E^c = 2.0$. The neutral surface locations have the same trend as in Fig. 3(a).

The effects of transverse isotropic parameter $S = G^*/G$ on K_{cr} and Z_n/h for circular plates are shown in Figs 4(a) and (b), where $R_0/h = 10$, $\beta = 0$ and E^t/E^c is equal to 0.2 and 2.0, respectively. It is seen that the larger the transverse isotropic coefficient S is, the greater the buckling load is, and the further

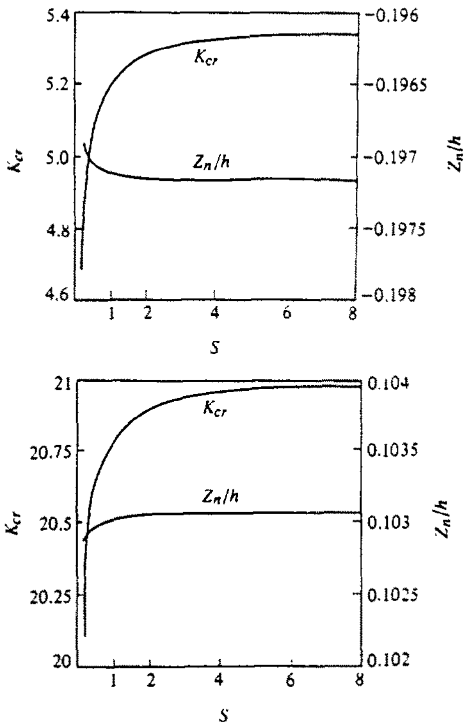

Fig. 4. Buckling coefficients and neutral surface locations of circular plate vs tranverse isotropic coefficients for (a) $E^t/E^c = 0.2$ and (b) $E^t/E^c = 2.0$. $R_0/h = 10$; $\beta = 0$.

the neutral surface location moves away from the midplane. Also, we can see that the effects of small S have more influences than those of large S. This means that the buckling load reduces and Z_n/h approaches the midplane when the transverse shear resistance is small.

Plots of E^t/E^c vs K_{cr} and Z_n/h for circular plates are shown in Fig. 5, where $R_0/h = 10$, $S = 1$ and $\beta = 0$. It is easy to be seen that the buckling coefficient K_{cr} increases with increasing the Young's modulus ratio E^t/E^c due to the larger values of rigidity as E^t/E^c increases, and the tensile zone decreases with increasing values of E^t/E^c.

Plots of K_{cr} vs β for circular plates are shown in Figs 6(a) and (b), with R_0/h and S equal to 10 and 1, respectively, and E^t/E^c equal to 0.2 and 2.0, respectively. The bending stress effects can be seen to reduce the buckling coefficient K_{cr} when $E^c/E^c < 1$ and increase it when $E^t/E^c > 1$. But the neutral surface location is shifted down when β is increased. Owing to the shifts of the neutral surface locations, the effects of bending stress on bimodulus materials have much more influence than those on ordinary materials (not bimodulus).

Figure 7 shows the neutral position Z_{nr}/h and $Z_{n\theta}/h$ of annular plates for two cases in which the ratios of

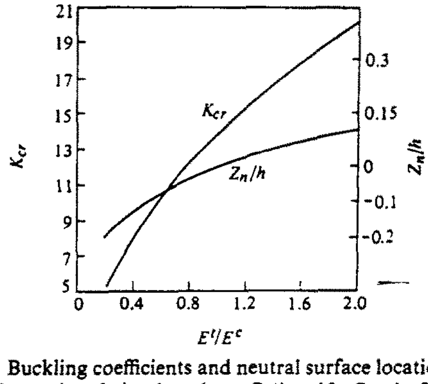

Fig. 5. Buckling coefficients and neutral surface locations vs modulus ratio of circular plate. $R_0/h = 10$; $S = 1$; $\beta = 0$.

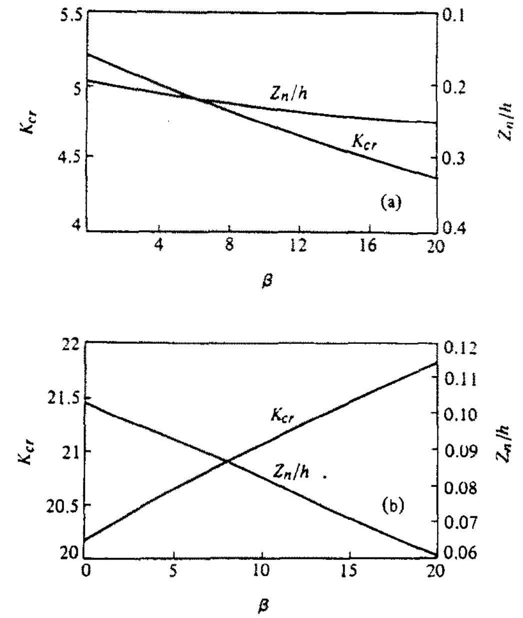

Fig. 6. Buckling coefficients and neutral surface locations vs bending stress ratio of circular plate for (a) $E^t/E^c = 0.2$ and (b) $E^t/E^c = 2.0$. $R_0/h = 10$; $S = 1$.

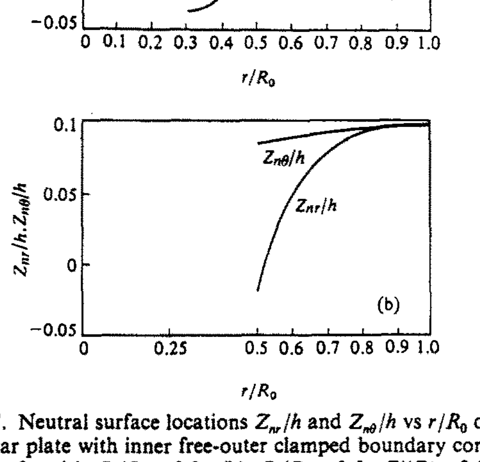

Fig. 7. Neutral surface locations Z_{nr}/h and $Z_{n\theta}/h$ vs r/R_0 of annular plate with inner free-outer clamped boundary condition for (a) $R_i/R_0 = 0.3$; (b) $R_i/R_0 = 0.5$. $E^t/E^c = 2.0$; $S = 1$; $\beta = 0$; $R_0/h = 10$.

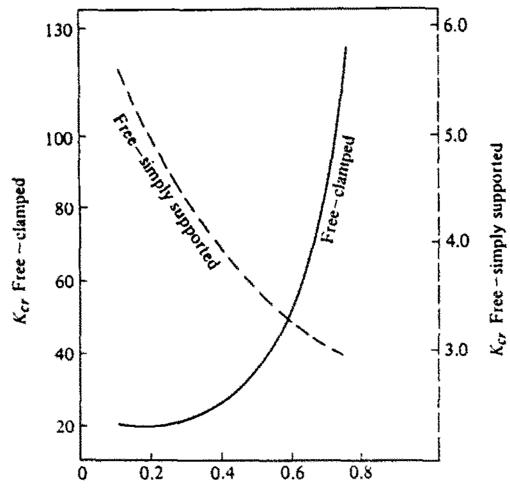

Fig. 8. Buckling coefficients K_{cr} of annular plates vs internal radius–external radius ratios R_i/R_0 of an annular plate with inner free–outer clamped boundary condition and with inner free–outer simply supported boundary condition for $E^t/E^c = 2.0$; $S = 0$; $\beta = 0$; $R_0/h = 10$.

internal radius to external radius R_i/R_0 are 0.3 and 0.5, respectively, where E^t/E^c, R_0/h, S and β are equal to 2.0, 10, 1 and 0, and their boundary conditions are free-clamped. The position Z_{nr} is derived by $\epsilon_{rr} = 0$ while $Z_{n\theta}$ is derived by $\epsilon_{\theta\theta} = 0$. It is seen that both Z_{nr} and $Z_{n\theta}$ vary with position and Z_{nr} is not the same as $Z_{n\theta}$ in general, and this phenomenon does not take place in cicular plates. It is believed that the Lame's distribution causes the result in the present study. We shall take the approach that $Z_n = \frac{1}{2}(Z_{nr} + Z_{n\theta})$ to solve the annular plates with isotropic bimodulus material. Even though this approach is rough, it provides an approach to complete this problem.

Plots of K_{cr} vs R_i/R_0 for annular plates are shown in Fig. 8, where E^t/E^c, R_0/h, S and β are equal to 2.0, 10, 1 and 0, respectively. The dashed line represents the buckling with free-simply boundary condition, while the solid line represents the buckling with free-clamped boundary conditon in Fig. 8. We can see that the buckling coefficient with free-clamped boundary condition has the lowest value when R_i/R_0 equals approximately 0.16. It is also seen that the buckling coefficients with free-simply boundary condition decrease with increasing the values of R_i/R_0 while the one with free-clamped condition has the reverse effect.

CONCLUSIONS

The following conclusions can be drawn from the preliminary results presented.

(1) The present finite strip method can produce accurate buckling analysis of a circular plate.

(2) The thicker the plate is, the lower the buckling coefficient K_{cr} is; the buckling loads $N_r(= hP_n)$ of thick circular plates are larger than those of thin circular plates.

(3) The buckling load increases with increasing transverse isotropic coefficient S. The effect can be seen more significantly when $S < 2$ for circular plates.

(4) The buckling load decreases with increasing initial bending stress coefficient for $E^t/E^c < 1$, and with decreasing β for $E^t/E^c > 1$ for circular plates.

(5) The buckling coefficient increases with increasing E^t/E^c for circular plates.

(6) The buckling of the annular bimodulus plates is also studied. The Lame's solution is found to have an important effect.

The buckling and vibration problems of laminated composite bimodulus circular plates need to be further studied. The results will be presented in the near future.

REFERENCES

1. S. K. Clark, The plane elastic characteristics of cord-rubber laminates. *Textile Res. J.* **33**, 295–313 (1963).
2. E. J. Seldin, Stress–strain properties of polycrystalline graphites in tension and compression at room temperature. *Carbon* **4**, 177–191 (1966).
3. S. A. Ambartsumyan and A. A. Khachatryan, The basic equations of the theory of elasticity for materials with different tensile and compressive stiffness. *Mech. Solids* **1**, 29–34 (1966).
4. C. W. Bert, Classical analysis of laminated bimodulus composite-material plates. University of Oklahoma, School of Aerospace, Mechanical and Nuclear Engineering, Contract No. N00014-78-C-0647 Report OU-AMNE-79-10A (1979).
5. C. W. Bert, Model for fibrous composites with different properties in tension and compression. *J. Engng Mat. Technol. ASME* **99H**, 344–349 (1979).
6. C. W. Bert, V. S. Reddy and S. K. Kincannon, Deflection of thin rectangular plates of cross-plied bimodulus material. *J. Struct. Mech.* **8**, 347–364 (1980).
7. J. N. Reddy and C. W. Bert, Analyses of plates contructed of fiber-reinforced bimodulus materials. *Mech. Bimodulus Mat. AMD* **33**, 67–83 (1979).
8. C. W. Bert, Bending of thick rectangular plates laminated of bimodulus materials. *AIAA J.* **19**, 1342–1349 (1981).
9. C. W. Bert, J. N. Reddy, W. C. Chao and V. S. Reddy, Vibration of thick rectangular plates of bimodulus composite material, *J. appl. Mech. ASME* **48**, 371–376 (1981).
10. N. Kamiya, Large deflection of a different modulus circular plate. *J. Engng Mat. Technol. ASME* **97H**, 52–56 (1975).
11. N. Kamiya, An energy method applied to large elastic deflection of a thin plate of bimodulus material. *J. Struct. Mech.* **3**, 317–329 (1975).
12. J. L. Doong and L. W. Chen, Axisymmetric vibration of an initially stressed bimodulus thick circular plate. *J. Sound Vibr.* **94**, 461–468 (1984).
13. E. J. Brunelle and S. R. Robertson, Initially stressed Mindlin plates. *AIAA J.* **12**, 1036–1044 (1974).
14. R. M. Jones, Buckling of circular cylindrical shells with different moduli in tension and compresion. *AIAA J.* **9**, 53–61 (1971).
15. R. M. Jones, Buckling of stiffened multilayered circular cylindrical shells with different orthotropic moduli in tension and compression. *AIAA J.* **9**, 917–923 (1971).
16. J. S. Przemieniecki, Finite element structural analysis of local instability. *AIAA J.* **11**, 33–39 (1973).
17. G. C. Pardoen, Static, vibration and buckling analysis

of axisymmetric circular plates using finite elements. *Comput. Struct.* **3**, 355–375 (1973).
18. G. C. Pardoen, Asymmetric vibration and stability of circular plates. *Comput. Struct.* **9**, 89–95 (1978).
19. M. N. Bapu Ras and K. S. S. Kumaran, Finite element analysis of Mindlin plates. *J. Mech. Des. ASME* **101**, 619–624 (1979).
20. S. Timoshenko and S. Woinowsky-Krieger, *Theory of Plates and Shells*, 2nd Edn. McGraw-Hill, New York (1959).
21. L. W. Chen and J. L. Doong, Vibrations of an initially stressed transversely isotropic circular thick plate. *Int. J. Mech. Sci.* **26**, 253–263 (1984).
22. Y. C. Fung, *Foundations of Solid Mechanics*, p. 114. Prentice-Hall, Englewood Cliffs, NJ (1965).
23. Y. K. Cheung, *Finite Strip Method in Structural Analysis*, p. 3 (1976).
24. J. L. Doong and L. W. Chen, Buckling of a bimodulus composite thick plate. Failure Prevention and Reliability Conference, ASME, pp. 95–200 (1983).

APPENDIX

$$\mathbf{E} = \begin{bmatrix} \frac{\partial}{\partial r} & 0 & 0 & 0 & 0 \\ \frac{1}{r} & \frac{1}{r}\frac{\partial}{\partial \theta} & 0 & 0 & 0 \\ \frac{\partial}{r\partial \theta} & \frac{\partial}{\partial r} - \frac{1}{r} & 0 & 0 & 0 \\ 0 & 0 & \frac{\partial}{\partial r} & 1 & 0 \\ 0 & 0 & \frac{1}{r}\frac{\partial}{\partial \theta} & 0 & 1 \end{bmatrix}$$

$$\mathbf{F} = \begin{bmatrix} 0 & 0 & 0 & \frac{\partial}{\partial r} & 0 \\ 0 & 0 & 0 & \frac{1}{r} & \frac{1}{r}\frac{\partial}{\partial \theta} \\ 0 & 0 & 0 & \frac{1}{r}\frac{\partial}{\partial \theta} & \frac{\partial}{\partial r} - \frac{1}{r} \\ 0 & 0 & 0 & 0 & 0 \\ 0 & 0 & 0 & 0 & 0 \end{bmatrix}$$

$$\mathbf{G}_1 = \begin{bmatrix} \frac{\partial}{\partial r} & 0 & 0 & 0 & 0 \\ \frac{1}{r}\frac{\partial}{\partial \theta} & -\frac{1}{r} & 0 & 0 & 0 \end{bmatrix}, \quad \mathbf{H}_1 = \begin{bmatrix} 0 & 0 & 0 & \frac{\partial}{\partial r} & 0 \\ 0 & 0 & 0 & \frac{1}{r}\frac{\partial}{\partial \theta} & -\frac{1}{r} \end{bmatrix}$$

$$\mathbf{G}_2 = \begin{bmatrix} 0 & \frac{\partial}{\partial r} & 0 & 0 & 0 \\ \frac{1}{r} & \frac{1}{r}\frac{\partial}{\partial \theta} & 0 & 0 & 0 \end{bmatrix}, \quad \mathbf{H}_2 = \begin{bmatrix} 0 & 0 & 0 & 0 & \frac{\partial}{\partial r} \\ 0 & 0 & 0 & \frac{1}{r} & \frac{1}{r}\frac{\partial}{\partial \theta} \end{bmatrix}$$

$$\mathbf{G}_3 = \begin{bmatrix} 0 & 0 & \frac{\partial}{\partial r} & 0 & 0 \\ 0 & 0 & \frac{1}{r}\frac{\partial}{\partial \theta} & 0 & 0 \end{bmatrix}, \quad \mathbf{H}_3 = \begin{bmatrix} 0 & 0 & 0 & 0 & 0 \\ 0 & 0 & 0 & 0 & 0 \end{bmatrix}.$$

The reduced material elastic constants are

$$\mathbf{Q} = \begin{bmatrix} \frac{E}{1-\nu^2} & \frac{\nu E}{1-\nu^2} & 0 & 0 & 0 \\ \frac{\nu E}{1-\nu^2} & \frac{E}{1-\nu^2} & 0 & 0 & 0 \\ 0 & 0 & G & 0 & 0 \\ 0 & 0 & 0 & k^2G^* & 0 \\ 0 & 0 & 0 & 0 & k^2G^* \end{bmatrix}$$